Practical and Intuitive Basis for Tensor Field Processing with Invariant Gradients and Rotation Tangents

Gordon L. Kindlmann and Carl-Fredrik Westin

Abstract Recent work has outlined a framework for analyzing diffusion tensor gradient and covariance tensors in terms of invariant gradient and rotation tangents, which span local variations in tensor shape and orientation, respectively. This chapter hopes to increase the adoption of this framework by giving it a more intuitive conceptual description, as well as providing practical advice for its numeric implementation. Example applications are described, with an emphasis on decomposing the third-order gradient of a diffusion tensor field.

1 Introduction

Diffusion tensor imaging (DTI) analysis aims to describe the complex and subtle architecture of white matter in the central nervous system based on multi-variate MRI measurements [3]. One of the challenges in tensor-valued image processing is determining how to handle the multiple degrees of freedom in each tensor sample. Many algorithms treat the coefficients of the tensor (as measured in the laboratory coordinate frame of the scanner) as channels in a multi-scalar image, similar to the independent color channels of an RGB image. The mathematics of tensor analysis, however, provide ingredients for designing tensor processing algorithms in a way that respects the biologically meaningful shape and orientation properties associated with the diffusion tensor.

The basic idea of this approach is to treat diffusion tensors as elements of a six-dimensional vector space, and to build at each tensor value $\mathbf{D}$ a coordinate system with three basis tensors (the *invariant gradients*) that span local variations in tensor shape, and three basis tensors (the *rotation tangents*) that span local variations in tensor orientation. This allows, for example, an edge detector to be sensitive to changes in anisotropy (part of tensor shape) but not fiber direction. Recent work [22]

Laboratory of Mathematics in Imaging, Brigham and Women's Hospital, Boston, Massachusetts, e-mail: gk|westin@bwh.harvard.edu

gives a detailed account of invariant gradients and rotation tangents, and the current chapter will not reproduce all the derivations. Rather, we hope here to give a better intuitive description of the method, to give more concrete information about how to implement it, and to provide an additional demonstration of its value for edge detection in tensor fields.

2 Mathematical Background

Describing our framework is easier with coordinate-free tensor expression. While it is always more concrete to represent tensors with their 3×3 matrix of coefficients, coordinate-free expressions can permit more concise derivations, and can also build on existing intuition about vector spaces and their bases. The notation reviewed here respects the difference between coordinate-free and coordinate-based expressions.

Our notation is summarized in Table 1, much of which is based on conventions of tensor analysis [10, 19]. A coordinate-free vector $\mathbf{v}$ has a representation in basis $\mathscr{B}$ as three coefficients $[v_1\, v_2\, v_3]^{\mathrm{t}} = v = [\mathbf{v}]_{\mathscr{B}}$ or just $[\mathbf{v}]$ where $\mathscr{B}$ is assumed. Each of the v_i coefficients is determined by $v_i = \mathbf{v} \cdot \mathbf{b}_i$. We use Einstein notation: a repeated index within a term implies summation over that index, *e.g.*, $[\mathbf{D}\mathbf{v}]_i = D_{ij} v_j = \sum_{j=1}^{3} D_{ij} v_j$; and $\mathbf{D} = D_{ij} \mathbf{b}_i \otimes \mathbf{b}_j = \sum_{i=1}^{3} \sum_{j=1}^{3} D_{ij} \mathbf{b}_i \otimes \mathbf{b}_j$.

This work starts with the recognition that tensors are linear transforms, and that linear transforms constitute a vector space. We stress these points because they appear infrequently in the tensor analysis commonly used for DTI. The tensor product $\mathbf{u} \otimes \mathbf{v}$ is a linear transform defined by $(\mathbf{u} \otimes \mathbf{v})\mathbf{w} = \mathbf{u}(\mathbf{v} \cdot \mathbf{w})$ for all vectors $\mathbf{w}$ [19]. Any linear transform $\mathbf{T}$ can be expressed as a linear combination of tensor products of orthonormal basis vectors $\mathbf{b}_i$, according to $\mathbf{T} = T_{ij} \mathbf{b}_i \otimes \mathbf{b}_j$ and $T_{ij} = \mathbf{b}_i \cdot \mathbf{T}\mathbf{b}_j$. Tensor contraction $\mathbf{A} : \mathbf{B}$ is an inner product on tensors. A *principal frame* $\mathscr{E} = \{\mathbf{e}_i\}$ is an orthonormal basis of eigenvectors of $\mathbf{D}$, which diagonalizes the matrix representation $[\mathbf{D}]_{\mathscr{E}} = diag(\lambda_1, \lambda_2, \lambda_3)$. The *spectral decomposition* $\mathbf{D} = \lambda_i \mathbf{e}_i \otimes \mathbf{e}_i$ is a coordinate-free expression of a tensor $\mathbf{D}$ in terms of its eigensystem.

While it is common to think of $\mathbf{D}$ as the covariance matrix of molecular displacements due to diffusion, it also revealing to recognize that a diffusion tensor $\mathbf{D}$ is a symmetric linear transform that maps (by Fick's first law) from concentration gradient vector ∇c to diffusive flux vector $\mathbf{j} = -\mathbf{D}\nabla c$ [12]. This fundamental property was pointed out by Basser in his original DTI work [3]. Diffusion tensors are also positive-definite [3], the significance of which for diffusion tensor image processing is discussed in Section 8.

Sym_3 is a six-dimensional vector space, as seen by forming an orthonormal basis $\mathscr{B} = \{\mathbf{B}_i\}_{i=1..6}$ for Sym_3 from an orthonormal basis $\mathscr{B} = \{\mathbf{b}_i\}_{i=1,2,3}$ for W.

Table 1 Mathematical Conventions and Notation

W	three-dimensional space
$W \otimes W$	three-dimensional second-order tensors
Sym_3	symmetric tensors in $W \otimes W$
SO_3	three-dimensional rotations
$\mathscr{B} = \{\mathbf{b}_i\}_{i=1,2,3}$	orthonormal basis for W
δ_{ij}	$\delta_{ij} = 1$ if $i = j$, 0 otherwise
$\mathbf{v}$	vector in W
$v = [\mathbf{v}]_{\mathscr{B}}$	matrix representation of $\mathbf{v}$ in $\mathscr{B}$; $v_i = \mathbf{v} \cdot \mathbf{b}_i$
$\mathbf{D}$	second-order tensor in Sym_3
$D = [\mathbf{D}]_{\mathscr{B}}$	matrix representation of $\mathbf{D}$ in $\mathscr{B}$; $D_{ij} = \mathbf{b}_i \cdot \mathbf{D}\mathbf{b}_j$
$\mathbf{I}$	identity tensor
$\mathbf{u} \otimes \mathbf{v}$	$\in W \otimes W$, tensor product of $\mathbf{u}$ and $\mathbf{v}$; $[\mathbf{u} \otimes \mathbf{v}]_{ij} = u_i v_j$
$\mathbf{A} : \mathbf{B}$	$= \mathrm{tr}(\mathbf{A}\mathbf{B}^{\mathrm{t}}) = A_{ij}B_{ij} \in \mathbb{R}$; contraction of $\mathbf{A}$ and $\mathbf{B}$
$\lvert\mathbf{A}\rvert$	$= \sqrt{\mathbf{A} : \mathbf{A}}$, tensor norm of $\mathbf{A}$, the Frobenius norm of matrix $[\mathbf{A}]$
$\overline{\mathbf{A}}$	$= \mathrm{tr}(\mathbf{A})\mathbf{I}/3$, isotropic part of $\mathbf{A}$
$\widetilde{\mathbf{A}}$	$= \mathbf{A} - \overline{\mathbf{A}}$, deviatoric part of $\mathbf{A}$
$\{\lambda_i\}, \{\mathbf{e}_i\}$	eigenvalues, eigenvectors of $\mathbf{D} = \lambda_i \mathbf{e}_i \otimes \mathbf{e}_i$; $\lambda_1 \geq \lambda_2 \geq \lambda_3$
$\{K_i\}, \{R_i\}$	orthogonal invariant sets; $K_1 =$ trace; $R_2 =$ FA; $K_3 = R_3 =$ mode
$\{\widehat{\boldsymbol{\nabla}_D K_i(\mathbf{D})}\}$	cylindrical invariant gradients, basis for shape variation around $\mathbf{D}$
$\{\widehat{\boldsymbol{\nabla}_D R_i(\mathbf{D})}\}$	spherical invariant gradients, basis for shape variation around $\mathbf{D}$
$\{\widehat{\boldsymbol{\Phi}_i(\mathbf{D})}\}$	rotation tangents, basis for orientation variation around $\mathbf{D}$
$\mathscr{G}$	third-order tensor in $\mathrm{Sym}_3 \otimes W$; matrix representation $G = [\mathscr{G}]$
$\mathbf{F}(\mathbf{x})$	tensor field; the DTI volume
$\mathbf{D} : \mathscr{G}$	$= D_{ij}G_{ijk}\mathbf{b}_k \in W$ contraction of $\mathscr{G}$ with $\mathbf{D}$
∇J	$= \boldsymbol{\nabla}_D J : \nabla\mathbf{F}$, spatial gradient of J in $\mathbf{F}$
$\nabla\widehat{J}$	$= \widehat{\boldsymbol{\nabla}_D J} : \nabla\mathbf{F}$, projected gradient of J
$\nabla\widehat{\phi_i}$	$= \widehat{\boldsymbol{\Phi}_i} : \nabla\mathbf{F}$, spatial "gradient" of $\mathbf{e}_i$ rotation

$$\left.\begin{array}{rcl} \mathbf{B_1} &=& \mathbf{b}_1 \otimes \mathbf{b}_1 \\ \mathbf{B_2} &=& (\mathbf{b}_1 \otimes \mathbf{b}_2 + \mathbf{b}_2 \otimes \mathbf{b}_1)/\sqrt{2} \\ \mathbf{B_3} &=& (\mathbf{b}_1 \otimes \mathbf{b}_3 + \mathbf{b}_3 \otimes \mathbf{b}_1)/\sqrt{2} \\ \mathbf{B_4} &=& \mathbf{b}_2 \otimes \mathbf{b}_2 \\ \mathbf{B_5} &=& (\mathbf{b}_2 \otimes \mathbf{b}_3 + \mathbf{b}_3 \otimes \mathbf{b}_2)/\sqrt{2} \\ \mathbf{B_6} &=& \mathbf{b}_3 \otimes \mathbf{b}_3 \end{array}\right\} \tag{1}$$

Tensors in Sym_3 can be decomposed into vector components by

$$\mathbf{D} = D_{\boldsymbol{i}}\mathbf{B}_{\boldsymbol{i}} = (\mathbf{D} : \mathbf{B}_{\boldsymbol{i}})\mathbf{B}_{\boldsymbol{i}}. \tag{2}$$

We use bold subscripts $\boldsymbol{i}$ to index components of Sym_3 considered as vectors rather than tensors. In addition to the coordinate-free description by (1), the treatment of

symmetric tensors as vectors can also be shown with matrix representations:

$$[\mathbf{D}]_{\mathscr{B}} = \begin{bmatrix} D_{\mathbf{1}} \\ D_{\mathbf{2}} \\ D_{\mathbf{3}} \\ D_{\mathbf{4}} \\ D_{\mathbf{5}} \\ D_{\mathbf{6}} \end{bmatrix} = \begin{bmatrix} D_{11} \\ \sqrt{2}D_{12} \\ \sqrt{2}D_{13} \\ D_{22} \\ \sqrt{2}D_{23} \\ D_{33} \end{bmatrix} \tag{3}$$

$$[\mathbf{D}]_{\mathscr{B}} = \begin{bmatrix} D_{11} & D_{12} & D_{13} \\ & D_{22} & D_{12} \\ \text{sym} & & D_{33} \end{bmatrix} = \begin{bmatrix} D_{\mathbf{1}} & D_{\mathbf{2}}/\sqrt{2} & D_{\mathbf{3}}/\sqrt{2} \\ & D_{\mathbf{4}} & D_{\mathbf{5}}/\sqrt{2} \\ \text{sym} & & D_{\mathbf{6}} \end{bmatrix}. \tag{4}$$

3 Conceptual Overview

As described in [22], a tensor $\mathbf{D}$ is rotated by $\mathbf{R}$ in SO_3 by

$$\psi(\mathbf{R},\mathbf{D}) = \mathbf{R}\mathbf{D}\mathbf{R}^{\mathrm{t}} \tag{5}$$

which changes the eigenvectors but not the eigenvalues (and hence not the *shape*) of $\mathbf{D}$. The *orbit* $\mathrm{SO}_3(\mathbf{D})$ of $\mathbf{D}$ is the set of all possible values of $\psi(\mathbf{R},\mathbf{D})$, that is, all reorientations of $\mathbf{D}$. Two tensors have the same shape if and only if they are on the same orbit. An *invariant* J is a scalar-valued function of tensors that is constant on orbits: ψ: $\mathrm{SO}_3(\mathbf{D}_0) = \mathrm{SO}_3(\mathbf{D}_1) \Rightarrow J(\mathbf{D}_0) = J(\mathbf{D}_1)$. Trace $\mathrm{tr}()$ and determinant $\det()$ are invariants, as are the eigenvalues, and any function of the eigenvalues.

We create *at each tensor* $\mathbf{D}$ a local orthonormal Sym_3 basis, with basis vectors (or "basis tensors") aligned with biologically meaningful degrees of freedom, namely *shape* and *orientation*. The tensor-valued *invariant gradients* are perpendicular to the orbits, and thus span local variations in tensor shape. The tangents to orbits, which we term *rotation tangents*, span local variations in tensor orientation, see Figure 1. In the following we develop expressions for the invariant gradients and

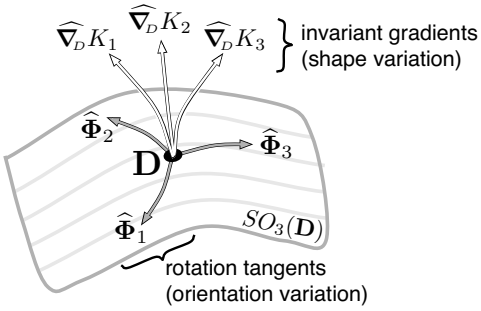

Fig. 1 Schematic view of degrees of freedom of shape and orientation variation around a given tensor $\mathbf{D}$. The tangents to the orbit $SO_3(\mathbf{D})$ (the rotation tangents, notated $\widehat{\mathbf{\Phi}}_i$) span variation in orientation around $\mathbf{D}$. The gradients of invariants (notated either $\widehat{\nabla}_D K_i$ or $\widehat{\nabla}_D R_i$ depending on the invariant set chosen) span variations in shape around $\mathbf{D}$.

rotation tangents that can be applied for practical operations. The full explanation for these derivations can be found in [22].

4 Invariant Gradients

Just as a scalar function defined over three-dimensional space has a vector-valued gradient that points in the direction of greatest increase, the gradient of a tensor invariant is a tensor-valued direction of fastest increase in the invariant. In terms of a first-order Taylor expansion [19],

$$J(\mathbf{D}_0 + \mathrm{d}\mathbf{D}) = J(\mathbf{D}_0) + \frac{\partial J}{\partial \mathbf{D}}(\mathbf{D}_0) : \mathrm{d}\mathbf{D} + O(\mathrm{d}\mathbf{D}^2) \tag{6}$$

$$\nabla_D J = \frac{\partial J}{\partial \mathbf{D}}. \tag{7}$$

We use ∇_D to denote the gradient of a function with respect to its tensor-valued argument (while gradients with respect to position in W are denoted by the usual ∇). Two invariants J_1 and J_2 are orthogonal if $\nabla_D J_1(\mathbf{D}) : \nabla_D J_2(\mathbf{D}) = 0$ for all $\mathbf{D}$, which intuitively means their level-sets are everywhere perpendicular.

Previous work has advocated two particular sets of three orthogonal invariants, notated K_i and R_i [15]

$$\begin{array}{ll} K_1(\mathbf{D}) = \mathrm{tr}(\mathbf{D}) & R_1(\mathbf{D}) = |\mathbf{D}| \\ K_2(\mathbf{D}) = |\widetilde{\mathbf{D}}| & R_2(\mathbf{D}) = \mathrm{FA}(\mathbf{D}) \\ K_3(\mathbf{D}) = R_3(\mathbf{D}) = \mathrm{mode}(\mathbf{D}) & . \end{array} \tag{8}$$

The mode invariant is [13]

$$\mathrm{mode}(\mathbf{D}) = 3\sqrt{6}\det(\widetilde{\mathbf{D}}/|\widetilde{\mathbf{D}}|). \tag{9}$$

The K_i and R_i invariant sets can be understood as cylindrical (K_i) or spherical (R_i) coordinate systems on the three-dimensional space of diagonal matrices ($D_{12} = D_{13} = D_{23} = 0$), centered on a central axis where $D_{11} = D_{22} = D_{33}$ [15]. We adopt these invariant sets because they naturally isolate biologically significant tensor attributes of size (tensor trace K_1 [28, 34] or norm R_1), amount of anisotropy (eigenvalue standard deviation K_2 or fractional anisotropy FA $= R_2$ [5, 24, 25, 33, 35]), and type of anisotropy (mode $K_3 = R_3$) [22]. Note that Trace (K_1) and FA (R_2) are not part of the same invariant set and are therefore not orthogonal, despite their common paired use as two complementary shape measures [20, 27].

The third invariant in both sets is *mode* [13]. Mode is a dimensionless parameter of anisotropy *type*, varying between -1 and +1, proportional to eigenvalue skewness [15]. Negative mode indicates planar anisotropy (oblateness, two large eigenvalues and one small eigenvalue); positive mode indicates linear anisotropy (prolateness, one large eigenvalue and two small). Fig. 2 illustrates the space spanned by tensor

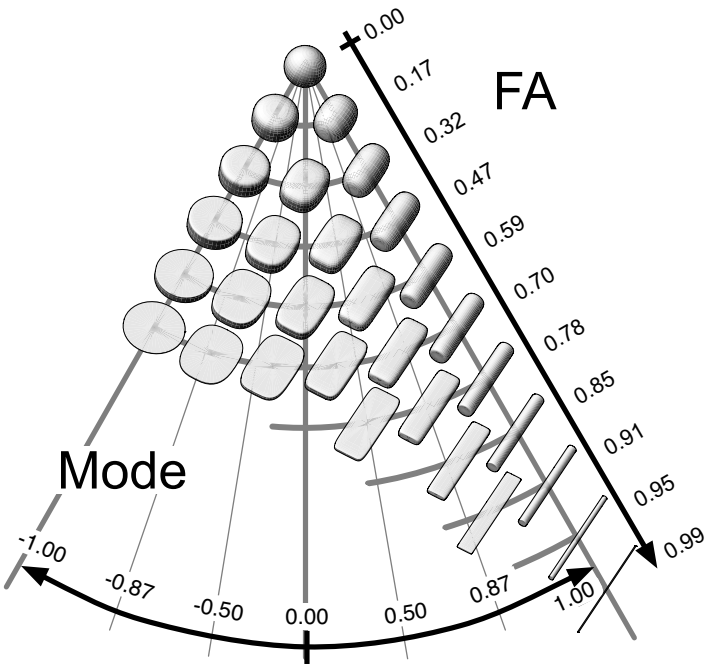

Fig. 2 Illustration of the bivariate space of FA $= R_2$ and Mode $= R_3 = K_3$ for tensors of fixed norm R_1. Tensors not shown (at high FA and negative mode) have negative eigenvalues.

mode and FA, using superquadric tensor glyphs [16]. Mode becomes less meaningful when K_2 or R_2 is low.

The tensor-valued gradients of K_i and R_i span local shape variations [15]:

$$\begin{aligned} \nabla_D K_1(\mathbf{D}) &= \mathbf{I} & \nabla_D R_1(\mathbf{D}) &= \mathbf{D}/|\mathbf{D}| \\ \nabla_D K_2(\mathbf{D}) &= \theta(\mathbf{D}) & \nabla_D R_2(\mathbf{D}) &= \sqrt{\tfrac{3}{2}}\left(\tfrac{\theta(\mathbf{D})}{|\mathbf{D}|} - \tfrac{|\widetilde{\mathbf{D}}|\mathbf{D}}{|\mathbf{D}|^3}\right) \\ \nabla_D K_3(\mathbf{D}) &= \nabla_D R_3(\mathbf{D}) = \tfrac{3\sqrt{6}\theta(\mathbf{D})^2 - 3K_3(\mathbf{D})\theta(\mathbf{D}) - \sqrt{6}\mathbf{I}}{K_2(\mathbf{D})} \end{aligned} \tag{10}$$

where $\theta(\mathbf{D}) = \widetilde{\mathbf{D}}/|\widetilde{\mathbf{D}}|$. To create elements of an orthonormal Sym_3 basis, we normalize the invariant gradients. $\widehat{\nabla_D} J$ denotes the unit-norm tensor-valued gradient of invariant J:

$$\widehat{\nabla_D} J(\mathbf{D}) = \nabla_D J(\mathbf{D})/|\nabla_D J(\mathbf{D})|\,. \tag{11}$$

These formulae obscure the fact that the numerical implementation of the invariant gradients is fairly simple. Finding the coefficients for the matrix representation of $\widehat{\nabla_D} K_1 = \nabla_D K_1$ and $\widehat{\nabla_D} R_1 = \nabla_D R_1$ is straightforward. With

$$[\widetilde{\mathbf{D}}]_{\mathscr{B}} = \begin{bmatrix} \frac{1}{3}(2D_{11} - D_{22} - D_{33}) & D_{12} & D_{13} \\ & \frac{1}{3}(2D_{22} - D_{11} - D_{33}) & D_{23} \\ \text{sym} & & \frac{1}{3}(2D_{33} - D_{11} - D_{22}) \end{bmatrix}, \tag{12}$$

$\widehat{\nabla_D} K_2 = \nabla_D K_2 = \widetilde{\mathbf{D}}/|\widetilde{\mathbf{D}}|$ is easily computed. Knowing that the magnitude of $\nabla_D R_2$ will be normalized to compute $\widehat{\nabla_D} R_1$, we can easily compute

$$\mathbf{E} = \sqrt{\frac{2}{3}}|\mathbf{D}|^2 \nabla_D R_2 = \frac{|\mathbf{D}|}{|\widetilde{\mathbf{D}}|}\widetilde{\mathbf{D}} - \frac{|\widetilde{\mathbf{D}}|}{|\mathbf{D}|}\mathbf{D} \tag{13}$$

and then $\widehat{\nabla_D} R_2 = \widehat{\nabla_D}\mathrm{FA} = \mathbf{E}/|\mathbf{E}|$. The formula for the remaining gradient $\nabla_D K_3 = \nabla_D R_3 = \nabla_D \mathrm{mode}$ is unwieldy, but it can be found by starting with the gradient of the determinant, which is is known from tensor analysis as [19]

$$\nabla_D \det(\mathbf{D}) = \det(\mathbf{D})\mathbf{D}^{-1}. \tag{14}$$

Subtracting out the components of $\nabla_D \det(\mathbf{D})$ parallel to $\widehat{\nabla_D} K_1$ and $\widehat{\nabla_D} K_2$ gives

$$\mathbf{G} = \nabla_D \det - (\nabla_D \det : \widehat{\nabla_D} K_1)\widehat{\nabla_D} K_1 - (\nabla_D \det : \widehat{\nabla_D} K_2)\widehat{\nabla_D} K_2 \tag{15}$$

which is simple to compute as a matrix given the equations above. It can be shown [23] that $\mathbf{G}$ vanishes only at the extremum of mode (where the gradient of mode vanishes anyway), so without loss of generality we can then define

$$\widehat{\nabla_D} K_3 = \mathbf{G}/\|\mathbf{G}\|. \tag{16}$$

which completes the numerical implementation of the normalized invariant gradients.

5 Rotation Tangents

The rotation tangents are defined in terms of the tensor eigenvectors $\{\mathbf{e}_1, \mathbf{e}_2, \mathbf{e}_3\}$, which are important for DTI applications. In nervous tissue, the principal eigenvector $\mathbf{e}_1$ is aligned with the direction of the white matter fiber tracts [9, 14, 32], which is the basis of most deterministic fiber tracking algorithms [7, 11].

Let $\mathbf{R}_\mathbf{v}(\phi) \in \mathrm{SO}_3$ be rotation by angle ϕ around $\mathbf{v}$. We define the *rotation tangent* $\boldsymbol{\Phi}_i(\mathbf{D})$ associated with eigenvector $\mathbf{e}_i$ of $\mathbf{D}$ as the change in tensor value due to infinitesimal rotations (5) around $\mathbf{e}_i$ [22]:

$$\boldsymbol{\Phi}_i(\mathbf{D}) = \left.\frac{\partial \psi(\mathbf{R}_{\mathbf{e}_i}(\phi), \mathbf{D})}{\partial \phi}\right|_{\phi=0} \Rightarrow \tag{17}$$

$$\boldsymbol{\Phi}_1(\mathbf{D}) = (\lambda_2 - \lambda_3)(\mathbf{e}_2 \otimes \mathbf{e}_3 + \mathbf{e}_3 \otimes \mathbf{e}_2)\,, \tag{18}$$

$$\boldsymbol{\Phi}_2(\mathbf{D}) = (\lambda_1 - \lambda_3)(\mathbf{e}_1 \otimes \mathbf{e}_3 + \mathbf{e}_3 \otimes \mathbf{e}_1)\,, \tag{19}$$

$$\boldsymbol{\Phi}_3(\mathbf{D}) = (\lambda_1 - \lambda_2)(\mathbf{e}_1 \otimes \mathbf{e}_2 + \mathbf{e}_2 \otimes \mathbf{e}_1)\,. \tag{20}$$

The rotation tangents $\boldsymbol{\Phi}_i(\mathbf{D})$ are mutually orthogonal, and all $\boldsymbol{\Phi}_i(\mathbf{D})$ are orthogonal to all invariant gradients [22].

The eigenvalue differences that scale the magnitude of the $\boldsymbol{\Phi}_i$ correspond to the intuition that if two eigenvalues are equal, then the tensor is rotationally symmetric, and there is no effect of rotating around its symmetry axis. To strengthen this intuition, for a tensor $\mathbf{D} = \lambda_i(\mathbf{e}_i \otimes \mathbf{e}_i)$ (spectral decomposition), we define $\mathbf{P} = \|\boldsymbol{\Phi}_i\|(\mathbf{e}_i \otimes \mathbf{e}_i)$ which has the same eigenvectors as $\mathbf{D}$, but has eigenvalues that reflect the magnitudes of the corresponding rotation tangents. These tensors are visualized in Figure 3(e). When $\mathbf{D}$ has rotational symmetry, either with linear or planar anisotropy (where mode K_3 is extremal), the orientation space of $\mathbf{D}$ is only two-dimensional (instead of three-dimensional), thus one eigenvalue of $\mathbf{P}$ is zero, and the $\mathbf{P}$ glyph is a flat disc. Note also that the overall size of $\mathbf{P}$ varies with anisotropy, as measured by K_2. Interestingly, although the space of orientation variation is in general three-dimensional, it is never isotropic: the $\mathbf{P}$ glyphs are never spheres (except at $\mathbf{P} = \mathbf{0}$). Thus, the $\mathbf{P}$ glyphs provide an general sense of how the space of orientation variation depends on tensor anisotropy and mode. The total number of degrees of freedom in the tensor is always six, but at rotational symmetries, the distinction between directions of shape variation and directions of orientation variation becomes blurred, as described in [22].

Unit-norm rotation tangents are defined as

$$\widehat{\boldsymbol{\Phi}}_1(\mathbf{D}) = (\mathbf{e}_2 \otimes \mathbf{e}_3 + \mathbf{e}_3 \otimes \mathbf{e}_2)/\sqrt{2} \tag{21}$$

$$\widehat{\boldsymbol{\Phi}}_2(\mathbf{D}) = (\mathbf{e}_3 \otimes \mathbf{e}_1 + \mathbf{e}_1 \otimes \mathbf{e}_3)/\sqrt{2} \tag{22}$$

$$\widehat{\boldsymbol{\Phi}}_3(\mathbf{D}) = (\mathbf{e}_1 \otimes \mathbf{e}_2 + \mathbf{e}_2 \otimes \mathbf{e}_1)/\sqrt{2}\,. \tag{23}$$

There are no simple matrix expressions for the $\widehat{\boldsymbol{\Phi}}_i$ in the laboratory frame because they depend on the tensor eigenvectors, but they are simple to create once the eigenvectors are found. Our approach for tensor analysis is the combination of normalized invariant gradients (either $\{\widehat{\nabla_D K_i}\}$ or $\{\widehat{\nabla_D R_i}\}$) and rotation tangents $\{\widehat{\boldsymbol{\Phi}}_i\}$, which together constitute an orthonormal Sym_3 basis, designed around a given tensor, to span the sub-spaces of shape and orientation variation.

6 Example Application: Edge Detection

With the machinery of invariant gradients and rotation tangents in place, one of the simplest applications is edge detection, based on measuring the spatial gradient

within the tensor data. Let $\mathbf{F}$ be a smooth tensor-valued image, or tensor field that represents DTI data:

$$\mathbf{F} : W \mapsto \mathrm{Sym}_3 \tag{24}$$

$$\mathbf{F}(\mathbf{x}) = \mathbf{D}. \tag{25}$$

The spatial gradient of $\mathbf{F}$ is a third-order tensor [19], previously described by Pajevic *et al.*, as part of their spline-based reconstruction [29]:

$$\begin{aligned} \nabla\mathbf{F} : W &\mapsto \mathrm{Sym}_3 \otimes W \\ \nabla\mathbf{F}(\mathbf{x}) &= \mathscr{G} \\ [\mathscr{G}]_{ijk} &= G_{ijk} = [\nabla\mathbf{F}(\mathbf{x})]_{ijk} = \left[\frac{\partial \mathbf{F}(\mathbf{x})}{\partial x_k}\right]_{ij} \end{aligned} \tag{26}$$

(26) describes how to compute the third-order gradient tensor; each D_{ij} in the matrix representation of the tensor is replaced by the spatial gradient of D_{ij} in the field.

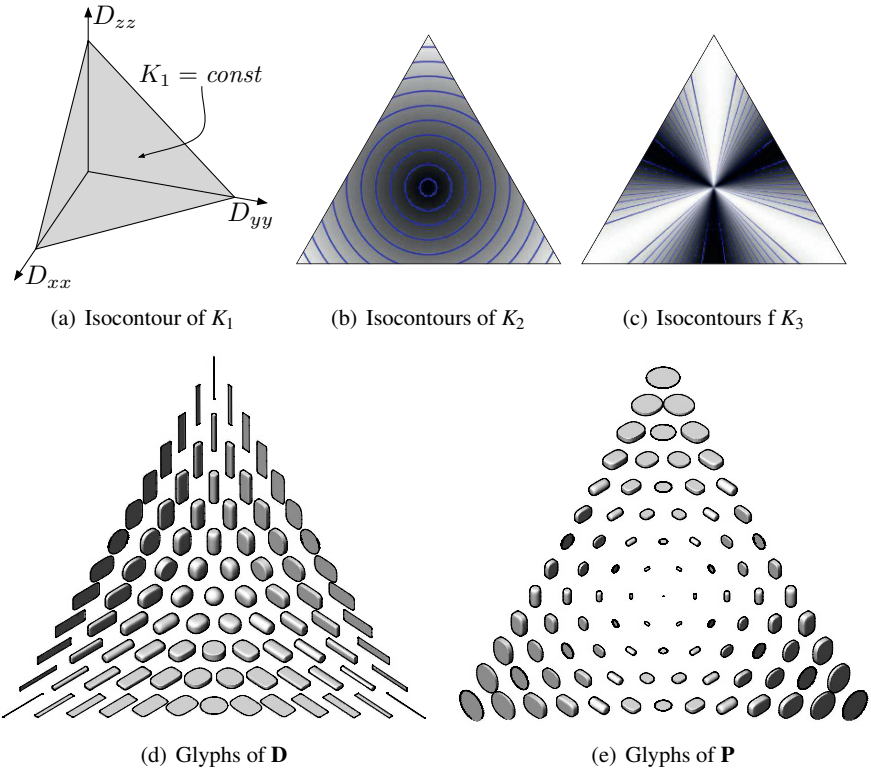

(a) Isocontour of K_1 (b) Isocontours of K_2 (c) Isocontours f K_3

(d) Glyphs of $\mathbf{D}$ (e) Glyphs of $\mathbf{P}$

Fig. 3 The space of effective orientation change in $\mathbf{D} = \lambda_i(\mathbf{e}_i \otimes \mathbf{e}_i)$, visualized by $\mathbf{P} = \|\boldsymbol{\Phi}_i\|(\mathbf{e}_i \otimes \mathbf{e}_i)$. Symmetries in $\mathbf{D}$ correspond to zero eigenvalues in $\mathbf{P}$.

Considering the coordinate-free representation, however, we see that the contraction of the full tensor gradient $\mathscr{G}$ with a fixed second-order tensor $\mathbf{T}$

$$\mathbf{T} : \mathscr{G} = \mathbf{T} : \nabla \mathbf{F}(\mathbf{x}) = \nabla (\mathbf{T} : \mathbf{F}(\mathbf{x})). \tag{27}$$

is the vector-valued gradient of the scalar $\mathbf{T} : \mathbf{F}(\mathbf{x})$. Thus, contractions of the gradient tensor $\nabla \mathbf{F}$ can access the differential structure of attributes of $\mathbf{F}$. Invariant gradients and rotation tangents provide the tensors with which we contract $\nabla \mathbf{F}$, generating three spatial gradient vectors of tensor shape, and three spatial gradients of tensor orientation.

Using the normalized invariant gradients, we define the *projected gradient* of invariant J in tensor field $\mathbf{F}$ by contracting $\nabla \mathbf{F}$ with the unit-norm $\widehat{\nabla_D J}$

$$\begin{aligned} \nabla \widehat{J} : W &\mapsto W \\ \nabla \widehat{J}(\mathbf{x}) &= \widehat{\nabla_D J}(\mathbf{F}(\mathbf{x})) : \nabla \mathbf{F}(\mathbf{x}) && (28) \\ &= \nabla_D J(\mathbf{F}(\mathbf{x})) : \nabla \mathbf{F}(\mathbf{x}) / |\nabla_D J(\mathbf{F}(\mathbf{x}))| && (29) \end{aligned}$$

$\nabla \widehat{J}$ is an abuse of notation to indicate normalization by tensor norm $|\nabla_D J|$, rather than vector length $|\nabla J|$; *i.e.*, $\nabla \widehat{J} \neq \widehat{\nabla} J$. $\widehat{\nabla_D J}$ differs from the regular spatial gradient of the invariant ∇J by a scaling factor that depends on the parameterization of J. By using normalized invariant gradients, the specifics of parameterization are removed. To numerically compute the projected invariant gradient of an invariant J, one first computes the 3×3 matrix $[\widehat{\nabla_D J}]$ (Sect. 4 describes this for $\widehat{\nabla_D K_i}$ and $\widehat{\nabla_D R_i}$), then computes the $3 \times 3 \times 3$ matrix $[\nabla \mathbf{F}]$ of the tensor field spatial derivative by finding the spatial gradient of each tensor coefficient D_{ij} (26). The project gradient is then found by contraction:

$$\begin{aligned} [\nabla \widehat{J}(\mathbf{x})]_k &= \widehat{\nabla_D J}(\mathbf{F}(\mathbf{x})) : \nabla \mathbf{F}(\mathbf{x}) \\ &= \sum_{i=1,2,3} \sum_{j=1,2,3} [\widehat{\nabla_D J}(\mathbf{F}(\mathbf{x}))]_{ij} [\nabla D_{ij}]_k && (30) \end{aligned}$$

Using the rotation tangents, we define three spatial gradients of orientation, one for each of the tensor eigenvectors

$$\begin{aligned} \nabla \widehat{\phi_i} : W &\mapsto W \\ \nabla \widehat{\phi_i}(\mathbf{x}) &= \widehat{\boldsymbol{\Phi}}_i(\mathbf{F}(\mathbf{x})) : \nabla \mathbf{F}(\mathbf{x}) \,. && (31) \end{aligned}$$

$\nabla \widehat{\phi_i}$ is also clearly an abuse of notation: there is no scalar field ϕ_i in which we can measure the spatial gradient. Rather, $\nabla \widehat{\phi_i}$ indicates the direction (in W) along which the tensor orientation "ϕ_i" around eigenvector $\mathbf{e}_i$ varies fastest. Indeed, this shows the utility of the rotation tangents: it allows the rate of rotation around eigenvector $\mathbf{e}_i$ to be isolated and measured, even though there is no global ϕ_i scalar quantity that represents the orientation around $\mathbf{e}_i$. The numerical computation of the orientation gradients is similar to that in (30).

To demonstrate this machinery for edge detection in a slice of a brain scan, Fig. 4 illustrates the tensor field gradient $|\nabla \mathbf{F}|$ and its decomposition along the invariant gradients and rotation tangents. Note that most of the gradient $\nabla \mathbf{F}$ is aligned along $\widehat{\nabla_D} R_1$, variation of tensor norm R_1, because of the large difference in diffusivity between the parenchyma (white and gray matter) and CSF. Previous work which

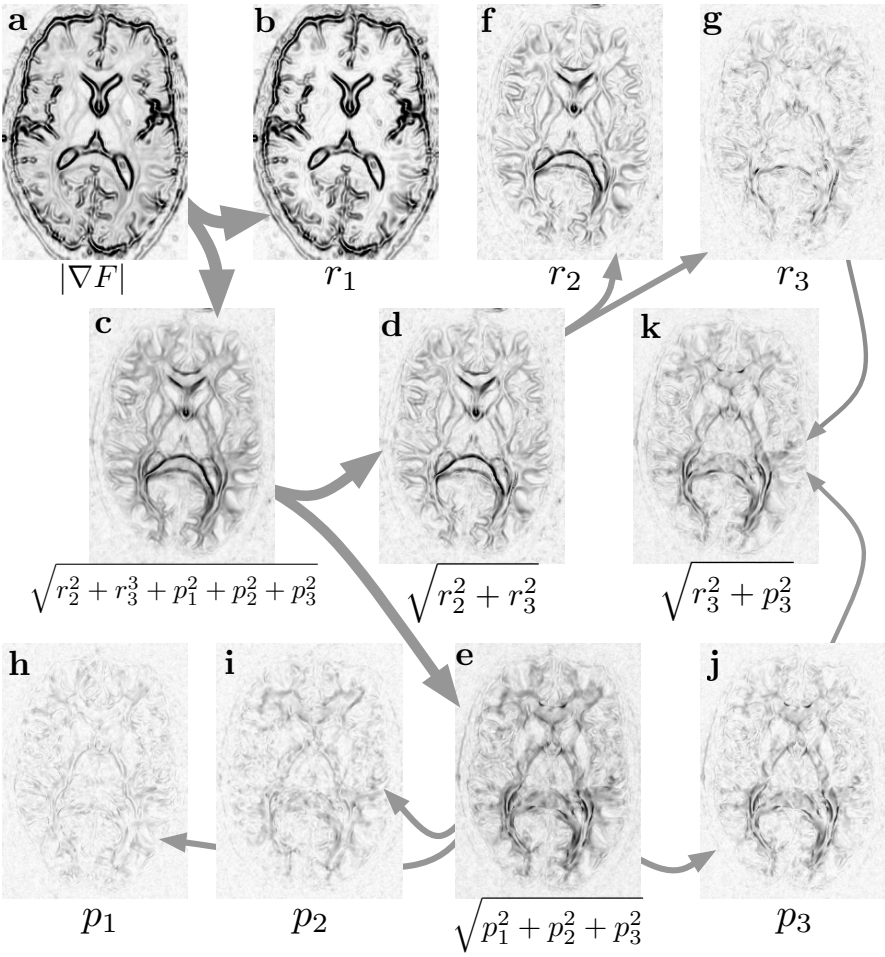

Fig. 4 Decomposition of tensor field gradient the magnitudes of the projected R_i invariant gradients $|\nabla \mathbf{F}|$ (a) with $r_i = |\nabla \widehat{R}_i|$, and the magnitudes of the orientation gradients $p_i = |\nabla \widehat{\phi}_i|$. Splitting r_1 (b) from the rest of the gradient (c) shows how most of the gradient is aligned with variation in tensor norm R_1, isolating the parenchyma-CSF boundary. Splitting (c) further, the remaining invariant gradients (d) capture tissue boundaries better than rotation tangents (e). The component along $R_2 = \text{FA}$ (f) in particular clearly shows the white matter boundary. The combination of $|\nabla \widehat{\phi}_3|$ (j) and $|\nabla \widehat{R}_3|$ (g) into (k) delineates white matter tracts that are adjacent yet distinctly oriented, such as between the cingulum bundle and corpus callosum, and between the tapetum, posterior corona radiata, and superior longitudinal fasciculus. Previous work terms (k) Adjacent Orthogonality [22].

introduced the study of tensor field gradients in DTI decomposed $\nabla\mathbf{F}$ into the gradient of the isotropic $\nabla\overline{\mathbf{F}}$ and deviatoric $\nabla\widetilde{\mathbf{F}}$ components, which is equivalent in our framework to separating out the component of $\nabla\mathbf{F}$ along $\widehat{\nabla_D K_1}$. Both trace K_1 and norm R_1 measure over-all size, so either will capture the CSF boundary. Our framework offers a more fine-grained decomposition of the gradient, enabling for example the Adjacent Orthogonality (AO) measure (Fig. 4(k)) that indicates locations where distinctly-oriented white matter pathways touch [22].

For comparison, Fig. 5 shows the decomposition of the tensor gradient in terms of the gradients of the individual tensor components, as measured in the $\mathscr{B}$ basis defined in (1).

The gradient components associated with the on-diagonal tensor coefficients emphasize the CSF boundary, while the gradients of off-diagonal coefficients do not, but the decomposition is not as specific as the decomposition along invariant gradients and rotation tangents, nor is it rotationally invariant. Comparing Figs. 4 and 5 supports our claim that the invariant gradients and rotation tangents offer a more biologically meaningful basis for tensor analysis.

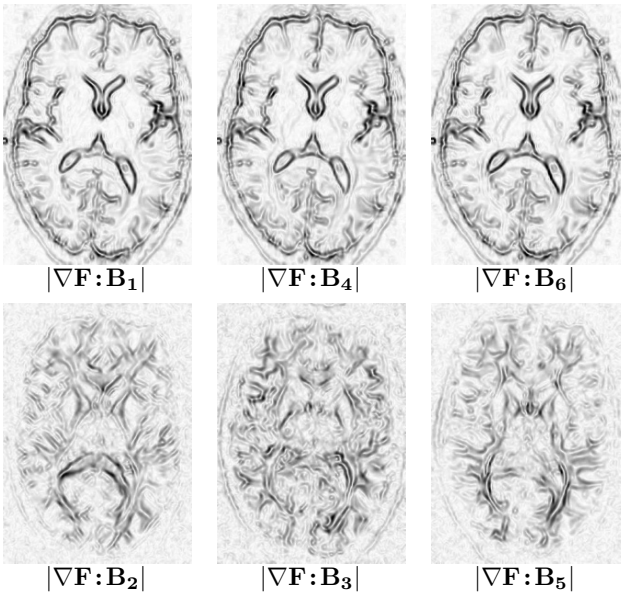

Fig. 5 Decomposition of tensor field gradient $|\nabla\mathbf{F}|$ with the $\mathscr{B}$ basis (1) corresponding to variation in the individual tensor components D_{ij}; compare to (4).

7 Other Applications

With the ability to selectively detect different kinds of tissue boundaries with the specialized edge detectors described above, one interesting application of invariant gradients and rotation tangents is to non-linear filtering of tensor fields. Just as Perona-Malik filtering [31] and most subsequent approaches to anisotropic (inhomogeneous) diffusion are based on a conductance function of a gradient magnitude, one can imagine a PDE-based tensor filtering algorithm that is based on a conductance function of some of the select edge components illustrated in Fig. 4. It might also be possible to restrict the updates to the per-sample tensor value according to variation in shape or orientation alone. Note also that the gradients in Fig. 4 are shown only as gradient *magnitudes*, but the gradient *vectors* also have spatial direction that is likely useful for describing the orientation of tissue interfaces.

Another application of the invariant gradients and rotation tangents is for the task of tensor interpolation. Previous work has described *geodesic-loxodromes* that are geodesics along tensor orientation orbits (Sect. 3), and loxodromes through variation of tensor shape [21]. These paths have the property that the angles between the interpolation path $\mathbf{P}(s)$ and three orthogonal invariant gradients (for example $\widehat{\nabla_D R_i}$) are constants c_i:

$$\frac{d\mathbf{P}}{ds} : \widehat{\nabla_D R_i} = c_i \ \forall i = 1,2,3. \tag{32}$$

One can also imagine, however, an interpolation path that is also a loxodrome in orientation, which obeys (32) as well as

$$\frac{d\mathbf{P}}{ds} : \widehat{\mathbf{\Phi}}_i = k_i \ \forall i = 1,2,3. \tag{33}$$

Along such a path, the rate of rotation around each eigenvector is constant. Investigations of such interpolation paths and their properties is ongoing.

8 Discussion

Our framework is "Euclidean" in that we consider diffusion tensors as elements of a vector space, even though this overlooks the positive-definiteness of diffusion. This simplifying assumption has established precedent in the DTI literature [4, 6, 7], even in the context of reconstructing tensors from discrete samples [1, 29]. In some approaches DTI analysis, tensors are located on a Riemannian manifold endowed with a metric that effectively creates an infinite distance between valid tensors and those with zero determinant [2, 8, 17, 18, 26, 30]. While these methods can leverage a wide range of Riemannian formalisms, we do not feel that the positive-definite constraint is a necessary ingredient for effective DTI processing, because we view the larger goals of image analysis (such as generating geometric models of anatomical features) as more important than maintaining the physical plausibility of the sam-

ple values at every stage in the analysis. By analogy, much work with traditional scalar-valued MR images use interpolation methods (*e.g.* windowed sinc) that do not necessarily preserve the positiveness of each pixel value, even though, as the magnitude of a complex-valued MR signal, it must be positive. We feel that the immediate practical utility of our tensor gradient decomposition (shown in Fig. 4) is adequate justification for our Euclidean approach to tensor analysis; the Riemannian methods have not produced a decomposition of the same specificity. We hope that invariant gradients and rotation tangents will provide a means of extending and creating a wide variety of image processing methods to tensor fields.

Acknowledgements This work supported by NIH grants NIBIB T32-EB002177, U41-RR019703, R01-MH074794, and NCRR P41-RR13218.

References

1. Akram Aldroubi and Peter Basser. Reconstruction of vector and tensor fields from sampled discrete data. *Contemporary Mathematics*, 247:1–15, 1999.
2. Vincent Arsigny, Pierre Fillard, Xavier Pennec, and Nicholas Ayache. Log-Euclidean metrics for fast and simple calculus on diffusion tensors. *Magnetic Resonance in Medicine*, 56(2):411–421, August 2006.
3. P J Basser, J Mattiello, and D LeBihan. Estimation of the effective self-diffusion tensor from the NMR spin-echo. *Journal of Magnetic Resonance, Series B*, 103(3):247–254, 1994.
4. P J Basser and S Pajevic. A normal distribution for tensor-valued random variables: Applications to diffusion tensor MRI. *IEEE Trans. on Medical Imaging*, 22(7):785–794, July 2003.
5. Peter J. Basser. Inferring microstructural features and the physiological state of tissues from diffusion-weighted images. *Nuclear Magnetic Resonance in Biomedicine*, 8:333–344, 1995.
6. Peter J. Basser and Sinisa Pajevic. Spectral decomposition of a 4th-order covariance tensor: Applications to diffusion tensor MRI. *Signal Processing*, 87:220–236, 2007.
7. Peter J. Basser, Sinisa Pajevic, Carlo Pierpaoli, Jeffrey Duda, and Akram Aldroubi. In vivo fiber tractograpy using DT-MRI data. *Magnetic Resonance in Medicine*, 44:625–632, 2000.
8. P. G. Batchelor, M. Moakher, D. Atkinson, F. Calamante, and A. Connelly. A rigorous framework for diffusion tensor calculus. *Magnetic Resonance in Medicine*, 53(1):221–225, January 2005.
9. C Beaulieu. The basis of anisotropic water diffusion in the nervous system-A technical review. *Nuclear Magnetic Resonance in Biomedicine*, 15:435–455, 2002.
10. D E Bourne and P C Kendall. *Vector Analysis and Cartesian Tensors*. CRC Press, 3rd edition, 1992.
11. Thomas E. Conturo, Nicolas F. Lori, Thomas S. Cull, Erbil Akbudak, Abraham Z. Snyder, Joshua S. Shimony, Robert C. McKinstry, Harold Burton, and Marcus E. Raichle. Tracking neuronal fiber pathways in the living human brain. *Proc. National Academy of Sciences*, 96:10422–10427, August 1999.
12. J Crank. *The Mathematics of Diffusion*. Oxford University Press, Oxford, England, 1975.
13. J C Criscione, J D Humphrey, A S Douglas, and W C Hunter. An invariant basis for natural strain which yields orthogonal stress response terms in isotropic hyperelasticity. *Journal of Mechanics and Physics of Solids*, 48:2445–2465, 2000.
14. Julien Dauguet, Sharon Peled, Vladimir Berezovskii, Thierry Delzescaux, Simon K. Warfield, Richard Born, and Carl-Fredrik Westin. 3D histological reconstruction of fiber tracts and direct comparison with diffusion tensor MRI tractography. In *Proceedings MICCAI 2006*, Lecture Notes in Computer Science 4190, pages 109–116, Copenhagen, Denmark, October 2006.

15. D B Ennis and G Kindlmann. Orthogonal tensor invariants and the analysis of diffusion tensor magnetic resonance images. *Magnetic Resonance in Medicine*, 55(1):136–146, 2006.
16. Daniel B. Ennis, Gordon Kindlman, Ignacio Rodriguez, Patrick A. Helm, and Elliot R. McVeigh. Visualization of tensor fields using superquadric glyphs. *Magnetic Resonance in Medicine*, 53:169–176, January 2005.
17. P Fillard, V Arsigny, X Pennec, and N Ayache. Clinical DT-MRI estimation, smoothing and fiber tracking with Log-Euclidean metrics. In *Proceedings ISBI 2006*, LNCS, pages 786–789, Arlington, Virginia, USA, April 2006.
18. P. Thomas Fletcher and Sarang Joshi. Principal geodesic analysis on symmetric spaces: Statistics of diffusion tensors. In *Proceedings ECCV 2004 Workshop on Computer Vision Approaches to Medical Image Analysis (CVAMIA)*, volume 31107 of *LNCS*, pages 87–98. Springer-Verlag, 2004.
19. G A Holzapfel. *Nonlinear Solid Mechanics*. John Wiley and Sons, Ltd, England, 2000.
20. Derek K. Jones, David Lythgoe, Mark A Horsfield, Andrew Simmons, Steve C. R. Williams, and Hugh S. Markus. Characterization of white matter damage in ischemic leukoaraiosis with diffusion tensor MRI. *Stroke*, 30:393–397, 1999.
21. G Kindlmann, RSJ Estépar, M Niethammer, S Haker, and C-F Westin. Geodesic-loxodromes for diffusion tensor interpolation and difference measurement. In *Proceedings MICCAI 2007*, Lecture Notes in Computer Science 4792, pages 1–9, Brisbane, Australia, October–November 2007.
22. Gordon Kindlmann, Daniel B. Ennis, Ross T. Whitaker, and Carl-Fredrik Westin. Diffusion tensor analysis with invariant gradients and rotation tangents. *IEEE Trans. on Medical Imaging*, 26(11):1483–1499, November 2007.
23. Gordon L Kindlmann. *Visualization and Analysis of Diffusion Tensor Fields*. PhD thesis, University of Utah, September 2004. `http://www.cs.utah.edu/$\sim$gk/PhD`.
24. T Klingberg, M Hedehus, E Temple, T Salz, J D E Gabrielli, M E Moseley, and R A Poldrack. Microstructure of temporo-parietal white matter as a basis for reading ability: Evidence from diffusion tensor magnetic resonance imaging. *Neuron*, 25:493–500, 2000.
25. M Kubicki, C-F Westin, S E Maier, H Mamata, M Frumin, H Ernst-Hirshefeld, R Kikinis, F A Jolesz, R W McCarley, and M E Shenton. Cingulate fasciculus integrity disruption in schizophrenia: A magnetic resonance diffusion tensor imaging study. *Biological Psychiatry*, 54:1171–1180, 2003.
26. C Lenglet, M Rousson, and R Deriche. DTI segmentation by statistical surface evolution. *IEEE Trans. on Medical Imaging*, 25:685–700, June 2006.
27. Stanley Lu, Daniel Ahn, Glyn Johnson, Meng Law, David Zagzag, and Robert I. Grossman. Diffusion-tensor MR imaging of intracranial neoplasia and associated peritumoral edema: Introduction of the tumor infiltration index. *Neuroradiology*, 232(1):221–228, July 2004.
28. M E Moseley, Y Cohen, J Mintorovitch, L Chileuitt, H Shimizu, J Kucharczyk, M F Wendland, and P R Weinstein. Early detection of regional cerebral ischemia in cats: Comparison of diffusion- and T2-weighted MRI and spectroscopy. *Magnetic Resonance in Medicine*, 14(2):330–346, May 1990.
29. S Pajevic, A Aldroubi, and P J Basser. A continuous tensor field approximation of discrete DT-MRI data for extracting microstructural and architectural features of tissue. *Journal of Magnetic Resonance*, 154:85–100, 2002.
30. Xavier Pennec. Probabilities and statistics on Riemannian manifolds: A geometric approach. Technical Report 5093, INRIA, Sophia Antipolis, January 2004.
31. Pietro Perona and Jitendra Malik. Scale-space and edge detection using anisotropy diffusion. *IEEE Transactions on Pattern Analysis and Machine Intelligence*, 12(7):629–639, 1990.
32. C Pierpaoli, P Jezzard, P J Basser, A Barnett, and G DiChiro. Diffusion tensor MR imaging of the human brain. *Radiology*, 201(3):637–648, Dec 1996.
33. S M Smith, M Jenkinson, H Johansen-Berg, D Rueckert, T E Nichols, C E Mackay, K E Watkins, O Ciccarelli, M Z Cader, P M Matthews, and T E J Behrens. Tract-based spatial statistics: Voxelwise analysis of multi-subject diffusion data. *NeuroImage*, 31:1487–1505, 2006.

34. C H Sotak. The role of diffusion tensor imaging in the evaluation of ischemic brain injury-A review. *Nuclear Magnetic Resonance in Biomedicine*, 15:561–569, 2002.
35. D S Tuch, D H Salat, J J Wisco, A K Zaleta, N D Hevelone, and H D Rosas. Choice reaction time performance correlates with diffusion anisotropy in white matter pathways supporting visuospatial attention. *Proc. National Academy of Sciences*, 102(34):12212–12217, 2005.